Optical design and evaluation of a three-dimensional imaging and ranging system based on time-correlated single-photon counting

John Massa, Gerald Buller, Andrew Walker, George Smith, Sergio Cova, Manickam Umasuthan, and Andrew Wallace

The design and operation of a noncontact surface profilometry system based on the time-correlated single-photon-counting technique are described. This system has a robust optomechanical design and uses an eye-safe laser that makes it particularly suitable for operation in an uncontrolled industrial environment. The sensitivity of the photon-counting technique permits its use on a variety of target materials, and its mode of operation does not require the continual presence of an operator. The system described has been optimized for a 1–25-m standoff, has a distance repeatability of <30 μm, and has a transverse spatial resolution of ~60 μm at a 2-m standoff and ~400 μm at a 13-m standoff.

OCIS codes: 010.4450, 290.5850, 290.4020.

1. Introduction

Time-correlated single-photon counting (TCSPC) is a statistical sampling technique that relies on the averaging of typically 10^5–10^6 individual measurements to provide a significant enhancement to the overall system timing accuracy. This technique has been employed for many years in time-resolved luminescence[1,2] and optical time-domain reflectometry[3] and uses instrumentation originally designed for use in nuclear counting experiments.

In a prior publication[4] we described the implementation of a time-of-flight (TOF) optical ranging system based on the TCSPC[5] technique. That prototype was used to test the feasibility of this technique for distance measurement and to determine the most suitable components and configuration for a future system. As it was intended for operation in a laboratory environment, it was designed to be flexible, permitting use of different components and configurations, at the expense of mechanical robustness and ease of use. On the basis of knowledge gained from this prototype, a second optimized system has now been built. This system has been designed to operate in an industrial environment over much longer distances, with a greatly increased depth of field and spatial resolution. Here we report use of this technique to provide three-dimensional (3-D) surface-profile maps of objects ranging from centimeters to meters in size.

Figure 1 shows a schematic diagram of the principal components of the improved TCSPC distance measurement system. To acquire full 3-D data, the optical head shown in Fig. 2 is mounted on a pan and tilt unit that is driven by X and Y stepper motors to give an angular accuracy of ~5 arc sec. This permits a minimum transverse step size of ~120 μm at a distance of 5 m, which is slightly less than the typical laser spot diameter as discussed in Section 3. An IBM-compatible PC is used to control both the stepper motors and an electronic driver unit that operates the laser, the detectors, and other components located inside the optical head. This eliminates the need for any manual adjustment or alignment when used in the field. Whereas the angular direction of the beam (and hence X and Y coordinates) is known

When this research was performed, J. Massa, G. Buller, A. Walker, and G. Smith were with Department of Physics, Heriot-Watt University, Riccarton, Edinburgh EH14 4AS, United Kingdom. J. Massa is now with Agilent Technologies, White House Road, Ipswich, Suffolk IP1 5PB, United Kingdom. S. Cova is with the Politecnico di Milano, Dipartmento di Elettronica e Informazione, Piazza Leonardo Da Vinci 32, 20133 Milano, Italy. M. Umasuthan and A. Wallace (andy@cee.hw.ac.uk) are with Heriot-Watt University, Department of Computing and Electrical Engineering, Riccarton, Edinburgh EH14 4AS, United Kingdom.

Received 20 February 2001; revised manuscript received 29 August 2001.

0003-6935/02/061063-08$15.00/0

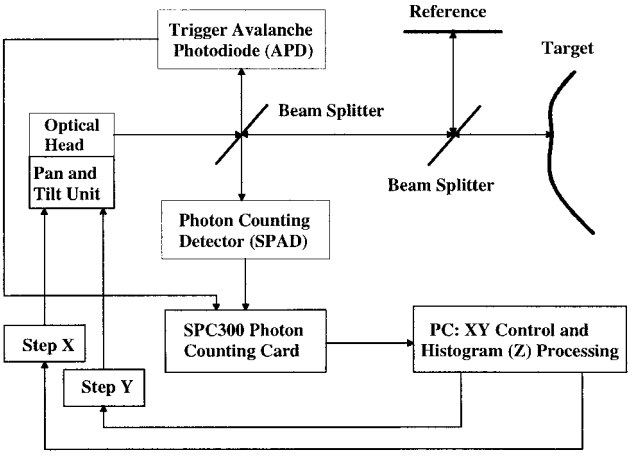

Fig. 1. Schematic diagram of the principal components of the TCSPC ranging system.

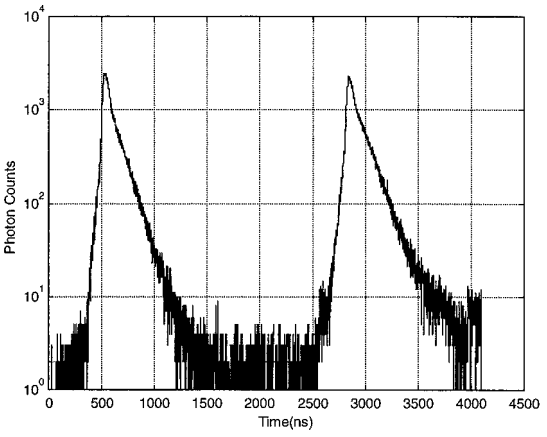

Fig. 3. Histogram of photon-count data. The target peak is on the left and the reference peak is on the right.

from the optical shaft encoders that are mounted on the pan and tilt head, the Z (range) measurement is computed from the measurement of the TOF of the laser beam to and from the target.

As shown in Fig. 1, a fraction of the source laser signal (~2%) is split off and directed toward a conventional analog avalanche photodiode (APD), which provides a trigger signal to start the timing system. The remaining laser signal is directed toward the target. The scattered return signal is collected and monitored with a photon-counting detector, a single-photon avalanche diode (SPAD) that provides a signal to the SPC-300 timing system. The time interval is then recorded before the system is reset. To faithfully record the target return pulse, the detection probability must be sufficiently low (typically <5%) to minimize any multiple photon events which will distort the statistical distribution of photon arrival times. By repetitively pulsing the laser, we can observe many photon timing events, and a histogram can be constructed that accurately represents the probability of photon arrival times and corresponds to the optical pulse shape in the time domain. In practice, to minimize the effect of drift in the timing electronics, a reference reflecting surface is added inside the optical head, together with suitable beam splitters, which causes a second pulse to appear on the recorded histogram, as shown in Fig. 3. Accurate distance measurements are made when we compare the timing of target returns relative to this reference signal.[6] Because TCSPC relies on the detection of the smallest quanta of optical energy, it follows that a system exploiting this technique will be far more light sensitive than conventional analog detection systems. This sensitivity has permitted measurements to be made from distant and arbitrary, i.e., uncooperative, targets by use of both minimal collection optics and an eye-safe laser. (Background light has not proven to be a problem and can be discriminated against by a wavelength-selective filter in front of the photon-counting detector.)

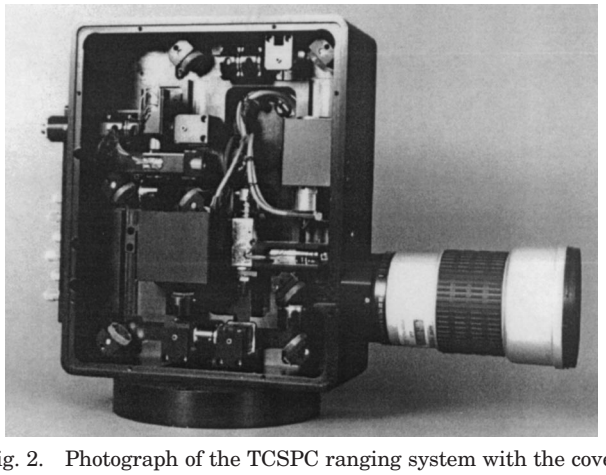

Fig. 2. Photograph of the TCSPC ranging system with the cover removed to show the layout of optical components on side (b) (see Fig. 5).

2. System Design

Schematic diagrams of the optical system layout are shown in Figs. 4 and 5. The components are arranged with the laser, trigger detector, and reference split off on one side of the central backplane (Fig. 4) and the SPAD, CCD camera, and mixing beam splitter together with the camera lens coupling optics on the other (Fig. 5). The layout minimizes the number of optical components shared by both the high-intensity laser output channel and the photon-counting channel. This decreases the number of stray optical reflections reaching the SPAD, which both simplifies the data analysis and reduces the time wasted by the photon-counting system responding to spurious signals. All optical components in the system, with the exception of the camera lens, are operating at an infinite conjugate ratio, with the laser output facet, SPAD, trigger detector, CCD camera, and fiber ends located in the respective focal planes of the various lenses.

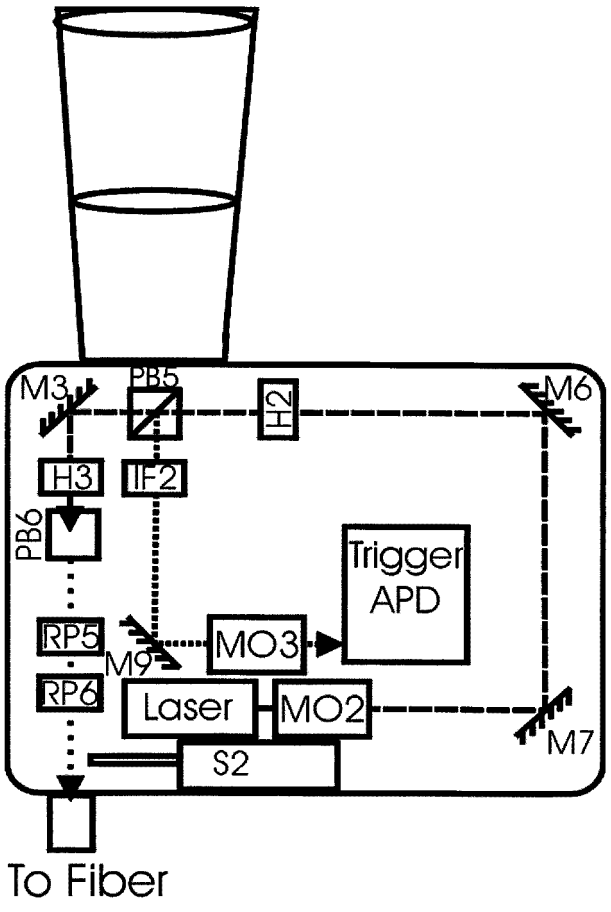

Fig. 4. Optical system layout of side (a) of the optimized TCSPC ranging system. M, mirror; H, half-wave plate; PB, polarizing beam splitter; RP, Risley prism; IF, interference filter; S, shutter solenoid; MO, microscope objective.

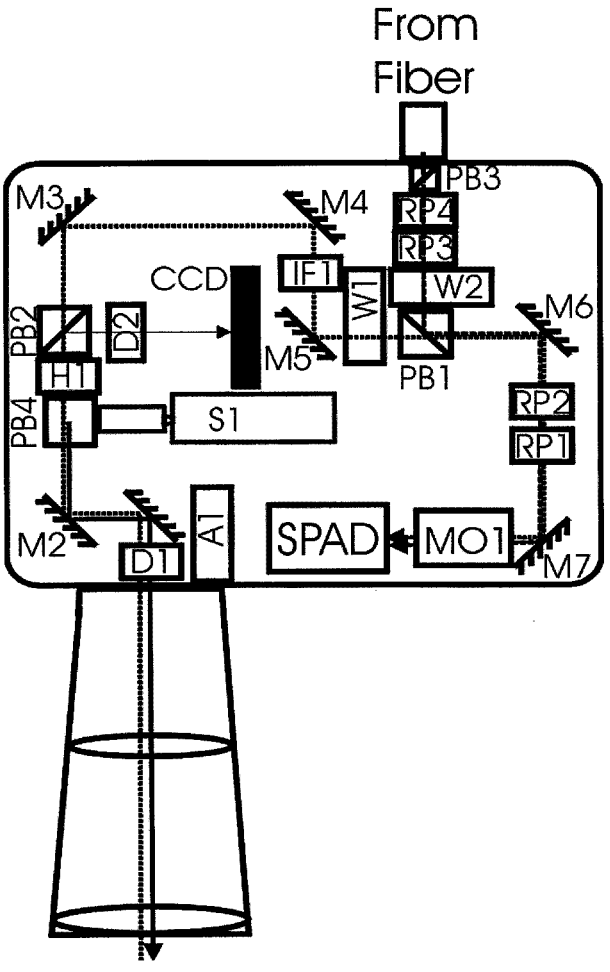

Fig. 5. Optical system layout of side (b) of the optimized TCSPC ranging system. M, mirror; H, half-wave plate; PB, polarizing beam splitter; RP, Risley prism; IF, interference filter; D, doublet; S, shutter solenoid; MO, microscope objective; W, stepper-motor-driven half-wave plate.

The optical head is formed from an aluminum alloy block of dimensions 260 mm × 210 mm × 100 mm that was machined to give recessed component bays on each side with a common central backplane. This forms a rigid structure for the mounting of the optical components but with minimal size and weight. The block is black anodized and has covers for each side to reduce the level of stray light entering the system and also to provide mechanical protection for the components. The layout of the system is defined by tracks machined into the surface of the central backplane that define an optical axis 10 mm above this level. The optical components, lenses, prisms, filters, and wave plates are mounted in steel cylinders of diameter 25 mm. In the previous laboratory system, the optical components were secured in position with magnets positioned along the tracks, which allowed continuous adjustment of the optical components along the axis. In this more rugged system, the components are secured to the backplane with fixed-position screws or clamps that allow only limited movement along the optical axis through elongated holes. We achieved rotation about the optical axis by fitting the components into lockable steel collars inside the 25-mm cylinders. The optical path inside the unit is folded numerous times by use of mirrors to make the system compact. The mirror mounts were designed to allow only limited movement, sufficient to compensate for manufacturing tolerances in the machining of the block.

The pulsed optical source used in this system is a passively Q-switched AlGaAs laser diode (developed at the Ioffe Institute, St. Petersburg) emitting 10–20-ps pulses and with energy ~7–10 pJ at a wavelength of 850 nm. This is driven at a repetition frequency of up to 25 MHz by an Avtech Model AVMH-3-C impulse generator. The low optical output from this laser (average power <0.25 mW) means that the system is eye safe and therefore can be used in an uncontrolled environment such as a factory floor or production line.

The photon-counting detector is an actively quenched silicon SPAD[7] that is capable of timing single-photon events with an accuracy of ~20 ps at a maximum count rate of several megahertz. Com-

pared with a photomultiplier tube, this detector exhibits a higher photon detection efficiency, a faster and cleaner time response,[8,9] and is far more robust for use in an industrial system. In addition, the detection of spurious reflections in the optical system is greatly reduced with this detector because its small active area, ~7 μm in diameter, spatially filters the optical signal in the detector plane. As a similar approach would be needed with any type of detector, the larger area of a photomultiplier tube is of no advantage.

In a conventional TCSPC system the pulsed electrical signals from the detectors are initially shaped with constant-fraction discriminators (CFDs). These CFDs provide a stable electrical output pulse with a temporal location that is invariant to changes in photon-count pulse amplitude. The precise timing of these signals is then accomplished with a time-to-amplitude converter (TAC) that produces an analog representation of the time interval between start and stop pulses. This signal is then digitized with an analog-to-digital converter (ADC) and stored in a multichannel analyzer. The CFDs and the TAC are normally situated in a stand-alone rack that provides the necessary stabilized power supplies for these units, whereas the ADC and multichannel analyzer are located on a card inside a PC. The maximum data throughput for such a system is normally limited to a few hundred kilohertz by the relatively long dead time of these electronic components. In a 3-D surface imaging system it is necessary to acquire distance measurements from as many points on the target as possible, over the shortest period of time. Thus, in this TOF system, where both compact and fast components are required, the CFDs, TAC, ADC, and multichannel analyzer were all integrated onto a single PC plug-in card (Becker & Hickle SPC-300) capable of a maximum data collection rate of several megahertz. The linearity and stability of this card were found to be comparable to systems based on conventional discrete components.

The laser is collimated by a ×10 microscope objective and routed by mirrors to a high-extinction ($>10^4$:1) polarizing beam splitter PB5 (Fig. 4). We set the polarization of the signal with respect to this beam splitter by rotating the laser about the optical axis. The total reflected signal (any *s*-polarized component from the laser and ~2% leakage from the *p* state) is focused onto the active area of the trigger APD with a ×5 microscope objective. Assuming a laser output facet size of ~2 μm, this gives an image size of ~4 μm on the 500-μm-diameter active area of the trigger APD.

The highly polarized signal transmitted through PB5 is *s* polarized with respect to PB6 and is predominantly reflected by the beam splitter through an aperture in the central backplane and emerges into the cavity on the other side. The transmitted signal at PB6 is of a sufficiently high level to supply the reference channel. To bring the reference pulse into the same time window as the target return, a fiber delay line is used (together with a separate beam combiner). We implement this by coupling the PB6 transmitted light into a single-mode polarization-maintaining fiber using a 9-mm focal-length lens and two Risley prism pairs, RP5 and RP6, for coarse and fine alignment.

The laser signal transmitted through the central backplane into the upper cavity is *s* polarized with respect to PB4 and thus is predominantly reflected toward the camera lens. A 25-mm focal-length doublet, D1, produces a focus in the back focal plane of the external camera lens. Thus it simultaneously couples the laser signal into the projection camera lens and transfers the collected scattered signal back into the detection channel. Currently, the camera lens used is a commercially available Pentax 200-mm *f*/2.8 telephoto, which is closely matched to the doublet to enable the full aperture of the camera lens to be used for both the outgoing and the return signals. The system was designed such that any lens utilizing the Pentax bayonet fitting can be used instead; however, some loss in signal will occur if the lens *f*-number is incorrectly matched.

The polarization state of the light incident on the target is linear; however, the state of the scattered signal is dependent on the nature of the surface. Polished metallic surfaces usually give a scattered signal that is predominantly the same polarization as the incident signal, whereas most other materials provide a signal that is elliptically polarized. Transmission of the return signal by PB4 discriminates against the laser polarization, and therefore a quarter-wave plate can be mounted at the front end of the camera lens to increase the signal from polished metal surfaces. This arrangement also ensures that any Fresnel reflection of the outgoing pulse from optical surfaces located between PB4 and the quarter-wave plate will be significantly attenuated by PB4 before reaching the SPAD detector.

The return signal, backscattered from the target, that is transmitted through PB4 is *p* polarized with respect to this beam splitter, and a half-wave plate H1 is used to rotate the polarization state of the signal incident on PB2 to ensure that it continues to be transmitted. The signal is then routed by mirrors, through interference filter IF1, centered at λ = 855 nm, which blocks out ambient light, and to the beam combiner PB1. The signal is *p* polarized with respect to PB1; however, the half-wave plate W1 can be rotated to adjust the fraction of the target signal transmitted to the detector. At PB1 it is combined with the reference signal that has passed through the polarization-maintaining fiber delay line. This reference signal is initially *p* polarized with respect to PB1 and is set when the fiber mount is rotated about the optical axis. The half-wave plate W2 can be adjusted to change the fraction of the reference signal reflected at PB1, toward the detector. PB1 has equal reflection and transmission extinction coefficients (>200:1) for *s*- and *p*-polarized light at 850 nm and thus allows equal attenuation of the target and reference signals of ~200:1 when the half-wave plates W1 and W2, respectively, are rotated. The

combined signals are then focused onto the SPAD with a ×10 microscope objective. Coarse and fine alignment of the target and reference signals onto the 7-μm-diameter SPAD is achieved by use of Risley prism pairs RP1 and RP2 for the target signal and RP3 and RP4 for the reference signal.

The optical system also contains a board-mounted CCD camera that provides an image of the target scene to aid in the positioning and calibration. Because PB4 is a broadband beam splitter, it transmits both polarizations in the visible region of the spectrum whereas the narrow-band PB2 reflects both polarizations in this wavelength region. The visible light collected by the external camera lens is therefore efficiently imaged, by doublet D2, onto the CCD sensor.

Four lengths of single-mode polarization-maintaining fiber (terminated by FC–PC connectors) are available for the reference arm: The lengths are 2.5, 5, 10, and 20 m. When we select combinations of these fibers, it is possible to create reference delays ranging from 8.75 to 131.25 ns in 8.75-ns increments. This is important because, to achieve the smallest-distance resolution from the system, it is necessary to have the TAC on the highest time resolution. Because the ADC resolution is limited to 12 bits, this leads to a restricted time window in which to observe the two signals; hence the target and reference pulses must arrive closely spaced in time. In practice, a compromise has to be made between distance accuracy and the depth of field that can be covered with a single fiber.

When we make relative distance measurements with a TOF system, it is desirable to be able to measure the temporal positions of the target and reference signals to a comparable precision. For our photon-counting system this is facilitated when we ensure a similar number of counts in the target and reference peaks of the histogram, which in turn implies similar intensities for these signals. The system was designed to actively control the optical signal incident on the SPAD detector by adjustment of the relative signal strengths in the target and reference channels. This is particularly important when highly structured surfaces are measured because the collected signal can vary by 3 orders of magnitude from one object point to the next. To achieve this control, the half-wave plates W1 and W2 were fitted with miniature stepper motors to permit automated adjustment of the target and reference signal levels reaching the detector. In addition, two solenoids S1 and S2 operate shutters in the target and reference channels to enable blocking of either signal. Finally, a stepper motor A1 is used to adjust the focus mechanism on the camera lens to ensure that the laser illumination on the target remains optimal. This combination of stepper motors and solenoids is used in conjunction with the feedback from the SPAD detector to provide dynamic control of all the signal levels in the system.

For a photon-counting system operating at a high data collection rate (>100 kHz), adjustment of the rate by rotation of the half-wave plates does not provide the usual $\sin^2(\theta)$ characteristic that is due to the nonlinear response associated with the finite dead time of the system components. The measured photon-count rate R_m is given by

$$R_m = \frac{1}{\tau}\left(1 - \exp\{-[R_T \sin^2(2\alpha_T) + R_R \sin^2(2\alpha_R)]\tau\}\right), \tag{1}$$

where R_T and R_R are the number of photons per second incident on the combining beam splitter (PB1) from the target and reference channels, respectively; and τ is the system dead time. α_T and α_R are the angles made by the fast or slow axes of the wave plates to the *s*- or *p*-polarization axes of PB1. From Eq. (1) the maximum possible collection rate $R_{\max}$ is given by

$$R_{\max} = \frac{1}{\tau}; \tag{2}$$

and when $R_T + R_R \ll R_{\max}$, the measured count rate as a function of angular position of the wave plates is simply

$$R_m = R_T \sin^2(2\alpha_T) + R_R \sin^2(2\alpha_R), \tag{3}$$

and the mark–space ratio is unity. As $R_T + R_R$ increases and becomes an appreciable fraction of $R_{\max}$, the peak signal rate asymptotically approaches the maximum signal rate and the mark–space ratio increases. In this TOF system the dead time of the signal processing electronics is ~350 ns, giving $R_{\max}$ = 2.86 MHz. Normally, to minimize pulse pileup, the maximum measured count rate would not be expected to exceed 1.5 MHz for a 25-MHz source repetition rate, which corresponds to $(R_T + R_R)\tau \sim 0.75$.

Figure 6 shows the theoretical wave-plate characteristic calculated from Eq. (1) for a system consisting of a single wave plate that was rotated through 180° and for values of $(R_T + R_R)\tau$ of 0.5, 1, 2, and 4. It is apparent that the characteristic is not sinusoidal and that its functional form changes with count rate. As a consequence of this effect, the complexity in the control of the target and reference signals when we use a pair of wave plates, one positioned in each channel, is considerably increased. A small decrease in the target signal level will not only reduce the number of processed events in this channel but will simultaneously lead to an increase in the number of events processed from the reference signal. Conversely, an increase in the target signal level will lead to a reduction in the number of events processed from the reference channel. Therefore we find it is necessary to calibrate the system, prior to making a scan, by determining R_R together with the fast and slow axis angles of the wave plates W1 and W2. With Eq. (1), R_T can then be determined from R_m, α_T, and α_R

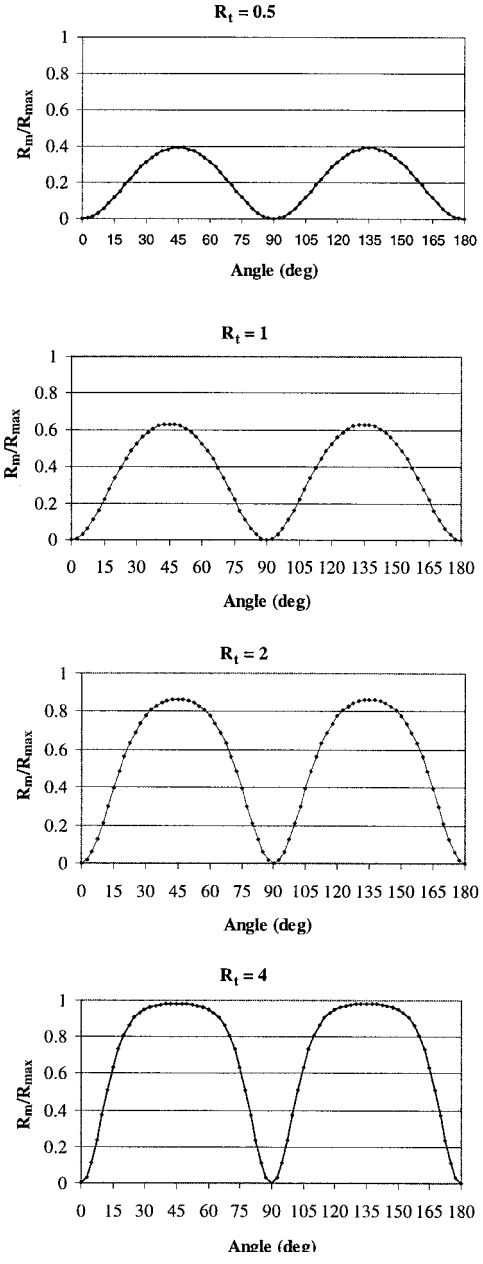

Fig. 6. Transmission characteristics of a half-wave plate and polarizer combination as measured with a photon-counting system operating at high dead time.

and an appropriate correction made to equalize the target and reference signals.

3. System Performance

In previous research,[4,10] as well as showing the high sensitivity of the TCSPC technique and the system stability, the distance measurement repeatability was demonstrated to be <30 μm and the lateral spatial resolution was <500 μm at distances of up to 5 m. The transverse spatial resolution of the system is determined by the laser spot size on the target. For the current system, the $1/e$ spot size ($FWe^{-1}M$) is ~ 60 μm $\times$ 170 μm at a distance of 2 m and a diameter of ~ 400 μm at a distance of 13 m. For a diffraction-limited system, the expected spot diameter would be ~ 60 μm at 2 m and ~ 380 μm at 13 m. Thus, as the angular repeatability of the pan and tilt platform is 5 arc sec, the depth accuracies of ~ 48 μm at a distance of 2 m and ~ 315 μm at 13 m are comparable to the spot sizes. One of the significant advantages of this approach to 3-D surface profiling, compared with those based on interferometric techniques, is the ability to automate the scanning process and thus allow dense imaging of large or complex surfaces without an operator being present. Figure 7(b) shows, as an example, a depth image of a university shield illustrated in Fig. 7(a) measured at a standoff distance of ~ 2 m with the TCSPC system. The image contains $\sim 6.8 \times 10^4$ data points (x, y, z measurements), each of which comprises an average of $\sim 5 \times 10^5$ single-photon events recorded at intervals of 1 s. The (x, y) sampling interval was 2 mm over the shield with a diameter of just over 50 cm. Hence the total scanning time was ~ 19 h. The dynamic range of the depth values in Fig. 7(b) is approximately 50 mm; each point in the displayed cloud of points is measured to a resolution of the order of 100 μm by the combined scanning and ranging system. For an alternative interferometric system, this object would have to be scanned interactively with an operator moving a retroreflecting sphere across the surface of the object. If the sphere contact point were lifted off the surface of the object (almost inevitable at the several step edges), then erroneous data would result, whereas if the beam is broken the system would have to be reinitialized. In addition, because such a system requires manual scanning, the density of the mesh of data points is generally nonuniform and ill-defined.

A further, commonly used, approach is based on triangulation. In this case the baseline distance must be increased to maintain the measurement accuracy as the standoff distance increases, making the system cumbersome. This method is also limited by occlusion effects. In addition, the sensitivity of such systems, when we are measuring difficult surfaces, is much inferior to the photon-counting method. Figure 8 shows another example, a computer reconstruction of a small model airplane scanned at a standoff distance of 1.26 m and at an angle of $\sim 20°$ to the vertical. This image has $\sim 1.4 \times 10^4$ data points acquired at a sampling interval of 1.5 mm. Whereas occlusion of many parts of this object causes missing data with triangulation, the TOF system, with its coaxial source and detector, produces a dense image, although the transparent cockpit causes difficulty. The mapped intensity values come from a photon-counting intensity image of the same model, clearly indicating the variation in signal intensity across the surface of the object because of the different surface reflectance. Because the system corrects for varying signal intensity, by either increasing integration time or attenuating the signal, an accurate 3-D sur-

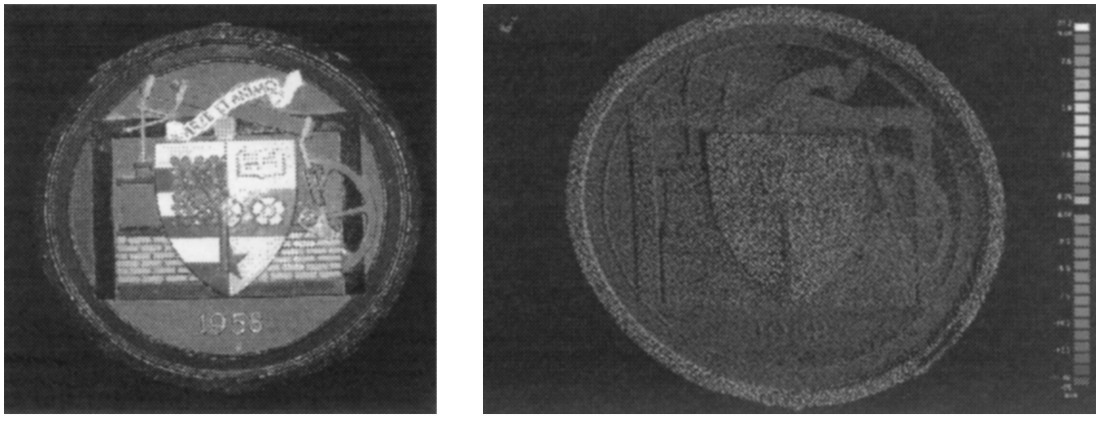

(a) (b)

Fig. 7. (a) Intensity image of a metallic shield showing the Heriot-Watt University crest. (b) Depth image of the shield obtained with the TCSPC system. The 3-D data are sampled at a spatial interval of 2 mm and contain $\sim 6.8 \times 10^4$ data points.

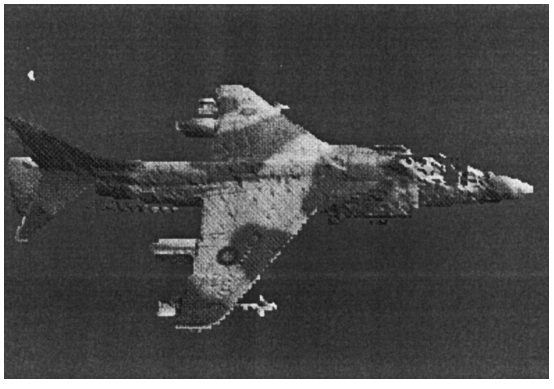

Fig. 8. Intensity mapped 3-D image of a model plane. The 3-D data are sampled at a spatial interval of 1.5 mm and contain $\sim 1.4 \times 10^4$ data points.

face contour can be measured independent of the surface albedo.

4. Conclusions

In this paper we have described and demonstrated the operation of a ruggedized turn key TOF surface profilometry and ranging system based on the TCSPC technique. The system has been operated at standoff distances in the range of 1–20 m and has been used to produce depth images of objects with sizes ranging from a few centimeters to several meters. The depth resolution of this system was previously demonstrated to be <30 μm,[4,10] and in this study a transverse spatial resolution of ~ 60 μm is reported at a distance of 2 m and ~ 400 μm at a distance 13 m.

Although data rates of one to three measurements per second were used to acquire the example scans presented, faster rates can be readily achieved at the cost of some sacrifice in depth resolution. These parameters relate to each other in the normal statistical fashion. Thus accepting a doubled-depth uncertainty, for example, permits a fourfold increase in the measurement rate. In addition there exists considerable potential to increase the basic photon-counting rate, which is currently limited by the timing electronics.

This study formed part of a collaboration between the authors with British Aerospace-Sowerby Research Centre and Edinburgh Instruments Ltd. and has been supported financially by the UK Engineering and Physical Sciences Research Council through their Integrated Machine Vision Initiative. The authors also acknowledge the financial support of the UK Royal Society Joint Project Fund, NATO Collaborative Research grant 9202218, and European Community International Association grant 93-2687. The passively *Q*-switched lasers were provided by E. L. Portnoi and co-workers, A. F. Ioffe Institute, St. Petersburg.

References

1. J. S. Massa, G. S. Buller, A. C. Walker, J. L. Oudar, E. V. K. Rao, B. G. Sfez, and R. Kuselewicz, "Evidence of carrier confinement in nonlinear GaAs/AlGaAs multiple quantum well microresonators fabricated using alloy mixing techniques," Appl. Phys. Lett. **61,** 2205–2207 (1992).
2. J. S. Massa, G. S. Buller, A. C. Walker, J. Simpson, K. A. Prior, and B. C. Cavenett, "Photoluminescence decay measurements of n- and p-type doped ZnSe grown by molecular beam epitaxy," Appl. Phys. Lett. **64,** 589–591 (1994).
3. G. Ripamonti, F. Zappa, and S. Cova, "Effects of trap levels in single-photon optical time-domain reflectrometry—evaluation and correction," J. Lightwave Technol. **10,** 1398–1402 (1992).
4. J. S. Massa, G. S. Buller, A. C. Walker, S. Cova, M. Umasuthan, and A. M. Wallace, "Time-of-flight optical ranging system based on time-correlated single-photon counting," Appl. Opt. **37,** 7298–7304 (1998).
5. D. V. O'Connor and D. Phillips, *Time-Correlated Single Photon Counting* (Academic, London, 1984).
6. M. Umasuthan, A. M. Wallace, J. S. Massa, G. S. Buller, and A. C. Walker, "Processing time-correlated single photon data to acquire range images," IEEE Proc. Vision Image Signal Process. **145**(4), 237–243 (1998).

7. S. Cova, M. Ghioni, A. Lacaita, C. Samori, and F. Zappa, "Avalanche photodiodes and quenching circuits for single-photon detection," Appl. Opt. **35,** 1954–1976 (1996).
8. A. Lacaita, M. Ghioni, and S. Cova, "Double epitaxy improves single-photon avalanche-diode performance," Electron. Lett. **25,** 841–843 (1989).
9. S. Cova, A. Lacaita, M. Ghioni, G. Ripamonti, and T. A. Louis, "20ps timing resolution with single photon avalanche diodes," Rev. Sci. Instrum. **60,** 1104–1110 (1989).
10. J. S. Massa, A. M. Wallace, G. S. Buller, S. J. Fancey, and A. C. Walker, "Laser depth measurement based on time-correlated single-photon counting," Opt. Lett. **22,** 543–545 (1997).